THEORETICAL AND EXPERIMENTAL STUDIES ON VISCOELASTIC PROPERTIES OF ERYTHROCYTE MEMBRANE

SHU CHIEN, KUO-LI PAUL SUNG, RICHARD SKALAK, SHUNICHI USAMI, and AYDIN TÖZEREN, *Department of Physiology, College of Physicians and Surgeons, and Department of Civil Engineering and Engineering Mechanics, College of Engineering and Applied Sciences, Columbia University, New York 10032 U.S.A., and Department of Engineering Sciences, Middle East Technical University, Ankara, Turkey*

ABSTRACT The deformation of a portion of erythrocyte during aspirational entry into a micropipette has been analyzed on the basis of a constant area deformation of an infinite plane membrane into a cylindrical tube. Consideration of the equilibrium of the membrane at the tip of the pipette has generated the relation between the aspirated length and the dimensionless time during deformational entry as well as during relaxation after the removal of aspiration pressure. Experimental studies on deformation and relaxation of normal human erythrocytes were performed with the use of micropipettes and a video dimension analyzer which allowed the continuous recording of the time-courses. The deformation consisted of an initial rapid phase with a membrane viscosity (range 0.6×10^{-4} to 4×10^{-4} dyn · s/cm) varying inversely with the degree of deformation and a later slow phase with a high membrane viscosity (mean 2.06×10^{-2} dyn · s/cm) which was not correlated with the degree of deformation. The membrane viscosity of the recovery phase after 20 s of deformation (mean 5.44×10^{-4} dyn · s/cm) was also independent of the degree of deformation. When determined after a short period of deformation (e.g., 2 s), however, membrane viscosity of the recovery phase became lower and agreed with that of the deformation phase. These results suggest that the rheological properties of the membrane can undergo dynamic changes depending on the extent and duration of deformation, reflecting molecular rearrangement in response to membrane strain.

INTRODUCTION

The biophysical properties of cell membranes are functional manifestations of their molecular organization and may play a significant role in influencing various types of cell activites. The membrane of erythrocytes has often been used as a model for studying the biophysical behavior of cell membranes, because of the relative ease of collection of these cells and existing knowledge on the molecular organization of erythrocyte membrane (Singer, 1974; Weissman and Clairborne, 1975). Furthermore, the viscoelastic properties of the erythrocyte membrane are of special interest due to the important role they play in influencing blood flow in health and disease (Chien, 1975; Skalak, 1976; Schmid-Schönbein, 1976).

Recent experimental and theoretical studies have shown that the viscoelastic behavior of the erythrocyte membrane varies with the mode of deformation. The elastic modulus of the membrane is several orders of magnitude higher during area expansion than in deformation at constant area (Skalak, 1973; Evans and Hochmuth, 1977). The widely different values of the elastic modulus of human erythrocyte membrane reported in the literature (Katchalsky et al., 1960; Rand, 1964; Hochmuth et al., 1973; Evans and LaCelle, 1975) have been incorporated into a single strain energy function consisting of two terms (Skalak et al., 1973; Evans, 1973*a*). One term gives the low elastic modulus observed when the membrane is deformed at constant area, and the other represents the high elastic modulus encountered when area increases.

Hoeber and Hochmuth (1970) and Evans and Hochmuth (1967*a*) have studied the time-course of the recovery of the aspirated portion of erythrocytes after their release from micropipettes. The time required for the aspirated segment to decrease its length by 50% is about 0.3 s. With the use of a two-dimensional Kelvin model and the assumption of area constancy, Evans and Hochmuth (1976*a*) have deduced that the data correspond to a surface membrane viscosity on the order of 10^{-3} dyn · s/cm. The time-course and the precise geometry of such recovery process after the erythrocyte has been expelled from the micropipette with a positive pressure, however, are difficult to quantify.[1] In the present investigations, experiments were designed to obtain quantitative data on the time-course of erythrocyte deformation during its aspirational entry into a micropipette and also that of erythrocyte recovery during the recession of the aspirated segment within the micropipette when the negative pressure is removed. The boundary constraint of the micropipette makes it possible to obtain geometric information in these studies. With the use of the viscoelastic constitutive equation of the membrane (Evans and Hochmuth, 1976*a*), theoretical analysis has developed solutions of the time history of the cell deformation and recovery in the micropipette. The combination of theoretical and experimental studies has led to the determination of membrane surface viscosity values not only during cell recovery, but also during deformation, which has not been heretofore investigated. The results reveal a complicated viscoelastic behavior of erythrocyte membrane.

THEORY

The following analysis of erythrocyte deformation in micropipette experiments is based on the aspiration of an infinite plane membrane into a cylindrical tube with radius R_p (Fig. 1). Cylindrical coordinates (R_o, Θ_o, Z_o) and (R, Θ, Z) denote the initial and deformed coordinates of the same material point in the membrane. It is assumed that the deformation occurs at a constant membrane surface area. Therefore, in the section of the membrane where $R \geq R_p$ and $Z = 0$, $\pi R_o^2 = \pi(R^2 - R_p^2) + \pi A$ or

$$R_o^2 = R^2 - R_p^2 + A, \tag{1}$$

[1] Recent studies by Hochmuth et al. (presented at 1977 American Institute of Chemical Engineers Meeting) on the recovery of erythrocytes with one end attached to a glass surface and the other end released from a micropipette have yielded a surface viscosity value of $6.0 \pm 0.2 \times 10^{-4}$ dyn · s/cm.

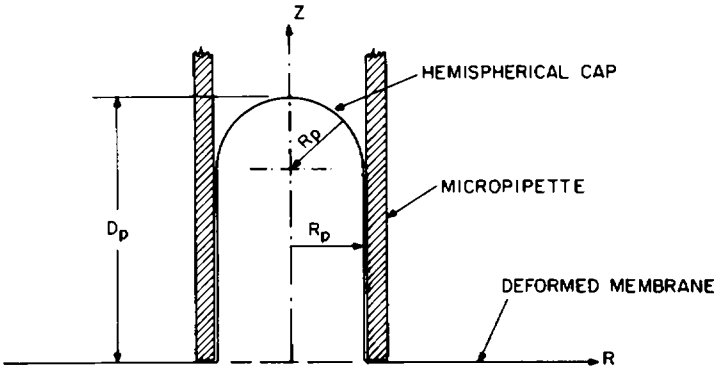

FIGURE 1 Schematic drawing of hemispherical cap model to show the coordinates (Z, R) for analyzing the aspiration of a portion of an infinite plane membrane into a cylindrical pipette with radius R_p.

where πA denotes the membrane surface area of the portion of the cell aspirated into the pipette, and it is a function of time (t). In the experiment, the length (D_p) of the portion of the cell in the micropipette is measured as a function of time. When D_p exceeds R_p, it is assumed that the aspirated portion consists of a hemispherical cap, with radius R_p, connected to a cylinder with radius R_p and length ($D_p - R_p$). Thus,

$$\text{for } D_p/R_p \geq 1, \qquad A = 2D_pR_p \tag{2}$$

$$\text{and} \qquad \dot{A} = 2R_p\dot{D}_p, \tag{3}$$

where $\dot{A}$ is the derivative of A with respect to time, keeping R_o constant. We have also treated small deformations with $D_p/R_p < 1$ by assuming that the portion of the cell in the micropipette takes on the shape of a spherical cap with various radii of curvature. Because of the involvement of significant bending stiffness, which is not included in the present treatment, analysis of such small deformations is given in the Appendix, and only the cases with $D_p/R_p \geq 1$ are considered here.

The stress analysis is carried out in the flat portion of the membrane ($R \geq R_p$). The extension ratio λ_1 in the radial direction is defined as the derivative of R with respect to R_o (i.e., final length ΔR divided by initial length ΔR_o). Using Eq. 1, λ_1 can be expressed as

$$\lambda_1 = (A + R^2 - R_p^2)^{1/2}/R. \tag{4}$$

Components of Green's strain tensor in this case are (assuming constant area, i.e., $\lambda_2 = 1/\lambda_1$):

$$\epsilon_{11} = (\lambda_1^2 - 1)/2 \tag{5a}$$

$$\epsilon_{22} = (\lambda_1^{-2} - 1)/2 \tag{5b}$$

where the direction of ϵ_{22} is meridonal.

The rate of strain V_{ij} is defined as the usual tensor used in viscous fluid theory

$$\frac{d}{dt}(ds^2 - ds_0^2) = 2V_{ij}dx_i dx_j, \tag{6}$$

where ds_o and ds denote the initial and deformed lengths of an infinitesimal material segment, and x_i are spatial coordinates. Components of the rate of strain tensor in this case[2] are

$$V_{11} = \dot{\lambda}_1/\lambda_1 = \dot{A}/2R^2 \tag{7a}$$

$$V_{22} = -\dot{\lambda}_1/\lambda_1 = -\dot{A}/2R^2, \tag{7b}$$

where $\dot{\lambda}_1$ is the derivative of λ_1 with respect to time, keeping R_o constant. Using a generalization of a Kelvin model (Evans and Hochmuth, 1976*a*, 1977), the following viscoelastic stress-strain relation of the erythrocyte membrane is assumed:

$$T_{ij} = -p\delta_{ij} + 2\mu\epsilon_{ij} + 2\eta V_{ij} \tag{8}$$

where T_{ij} is membrane tension, $(-p)$ is the pressure term due to constant surface area, μ is the coefficient of elasticity,[3] and η is the coefficient of viscosity. Using Eqs. 5 and 7, T_{11} and T_{22} can be written as:

$$T_{11} = -p + \mu\{[(A + R^2 - R_p^2)/R^2] - 1\} + \eta\dot{A}/R^2 \tag{9}$$

$$T_{22} = -p + \mu\{[R^2/(A + R^2 - R_p^2)] - 1\} - \eta\dot{A}/R^2. \tag{10}$$

Now it is assumed that R_{11} at the edge of the pipette is continuous. The tension T_{11}^0 in Z direction at the tip of the pipette is:

$$T_{11}^0 = R_p\Delta P/2, \tag{11}$$

where ΔP denotes the pressure difference between the cell and the pipette and is assumed to be equal to the applied aspiration pressure. The membrane is assumed to slide freely at the tip of the pipette so that the tensions are continuous. Consideration of equation of equilibrium of the flat membrane in R direction requires

$$T_{11} - T_{22} + R(dT_{11}/dR) = 0. \tag{12}$$

T_{11}^0 can then be expressed as:

$$T_{11}^0 = \int_{R_p}^{\infty} (T_{11} - T_{22})dR/R. \tag{13}$$

Using Eqs. 9 and 10, Eq. 13 can be integrated to give:

$$T_{11}^0 = (\mu/2)\{[(A - R_p^2)/R_p^2] + \ln(A/R_p^2)\} + \eta(\dot{A}/R_p^2). \tag{14}$$

[2]The constitutive equation proposed by Evans and Hochmuth (1976*a*, 1977) is used here. Chien (1977) has proposed a different relation. At the present time, there is insufficient information to establish which relation should be employed. We decided to use the equation proposed by Evans and Hochmuth so that the results can be compared readily with theirs.

[3]The coefficient of elasticity used in this paper is equal to one-half of the elastic modulus originally defined by Evans (1973*a*).

Let $x = D_p/R_p$. Substitution of Eqs. 2, 3, and 11 into Eq. 14 yields:

$$(\Delta p)R_p/\mu = (2x - 1 + \ln 2x) + 4\tau\dot{x}, \tag{15}$$

where τ is the time constant:

$$\tau \equiv \eta/\mu. \tag{16}$$

Let D_{pm} denote the maximum, steady-state value of D_p obtained after the application of a step aspiration pressure. For this steady-state equilibrium position, when x_m is reached, $\dot{x}$ becomes zero. Hence

$$(\Delta P)R_p/\mu = (2x_m - 1 + \ln 2x_m). \tag{17}$$

The time required to reach a given x is solved by combining Eqs. 15 and 17:

$$t = \tau \int_1^x \frac{dx}{F(x)} \tag{18}$$

where

$$F(x) = [2(x_m - x) + \ln(x_m/x)]/4. \tag{19}$$

Eq. 18 indicates that, according to the two-dimensional Kelvin model, the time-dependent deformation process in response to a step aspiration pressure can be described by the use of the dimensionless time $(t - t_1)/\tau$, where t_1 is the time at which $x = 1$.

Eq. 17 describes the relation between the steady-state deformation (x_m) and the dimensionless membrane tension $[(\Delta P)R_p/\mu]$. As shown in Fig. 2, the results computed from the present theory with a spherical cap model agree well with the results of Evans' theory (1973). The derivation of the present theory for $x_m < 1$ is given in the Appendix. Fig. 2 indicates that, when $x_m > 1$, the relation between x_m and $(\Delta P)R_p/\mu$ is approximately linear:

$$(\Delta P)R_p/\mu = ax_m + b. \tag{20}$$

For D_{pm}/R_p over a range of 1 to 4, Eq. 20 can be fitted with $a = 2.45$ and $b = -0.603$. Using Eq. 15,

$$ax_m + b = ax + b + 4\tau\dot{x}. \tag{21}$$

Integrating Eq. 21 gives an approximation for t:

$$t - t_1 = (4/a)\tau \ln[(x_m - 1)/(x_m - x)], \tag{22}$$

where t_1 is the time at which $x = 1$, and $4/a = 1.633$. Points computed by this approximate solution (Eq. 22) are shown superimposed on the results of Eqs. 18 and 19, with very good agreement (Fig. 3). This approximate form is useful in examining the experimental data to see if it can be fitted by a Kelvin model, as Eq. 22 can be written

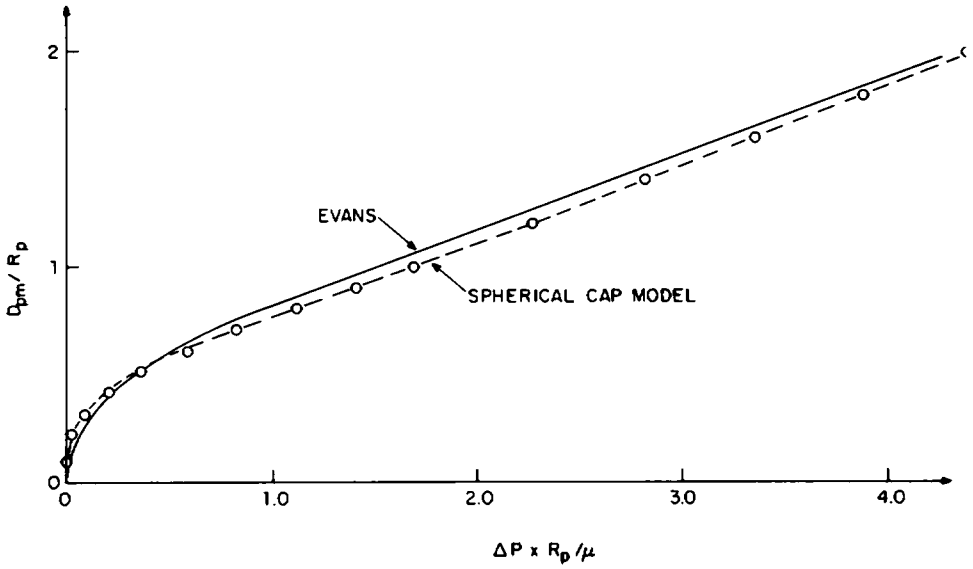

FIGURE 2 Steady-state dimensionless deformation (D_{pm}/R_p) as a function of dimensionless membrane tension [$(\Delta P)R_p/\mu$] obtained by the present theory with a spherical cap model, showing good agreement with the results of Evan's theory (1973*b*).

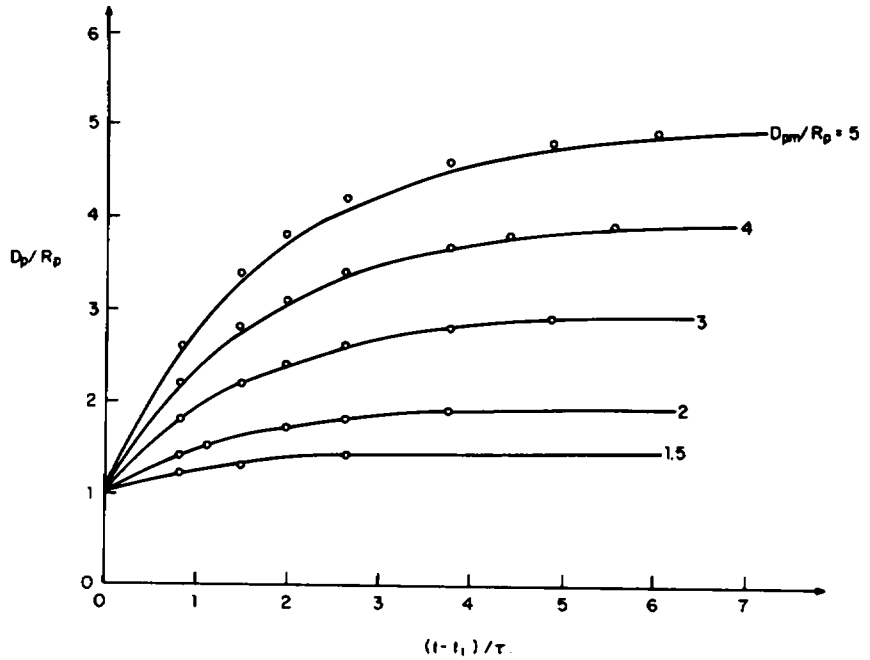

FIGURE 3 Theoretical modeling of time-dependent deformation of erythrocytes into the micropipette. Dimensionless deformation (D_p/R_p) as a function of dimensionless time $(t - t_1)/\tau$, where t_1 is the time at which $D_p/R_p = 1$. A family of curves with the steady-state dimensionless deformation (D_{pm}/R_p) up to 5 are shown. Solid curves are obtained by integration (Eqs. 18 and 19). Circles are computed by approximate Eq. 23.

as:

$$(x_m - x)/(x_m - 1) = e^{-(t-t_1)/1.633\tau} \tag{23}$$

The relaxation of the aspirated cell segment inside the micropipette is brought about by suddenly removing the aspiration pressure. The differential equation governing the relaxation phase can be obtained by setting the tension T_{11}^0 in Eq. 14 to zero and substituting Eq. 2 into Eq. 14. For $x \geq 1$,

$$\frac{\mu}{2}(2x - 1 + \ln 2x) + 2\eta\dot{x} = 0. \tag{24}$$

Integrating Eq. 24:

$$t = \tau \int_x^{x_m} \frac{dx}{G(x)}, \quad 1 \leq x \leq x_m \tag{25}$$

where

$$G(x) = (2x - 1 + \ln 2x)/4. \tag{26}$$

The relaxation curves computed from the above considerations are plotted in Fig. 4. Unlike the loading curves, the relaxation curves for different x_m values can be reduced to one single curve (Fig. 5; see Appendix for the portion of the curve with $x < 1$).

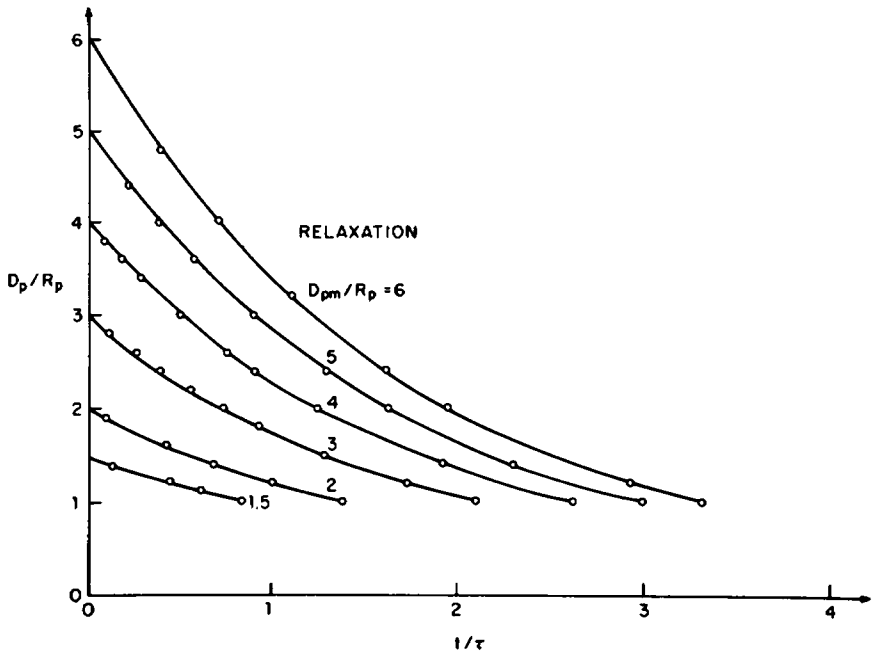

FIGURE 4 Theoretical modeling of relaxation of erythrocytes in the micropipette. A family of curves with D_{pm}/R_p up to 6 are shown. Solid curves are obtained by integration (Eqs. 25 and 26). Circles are computed by Eq. 30.

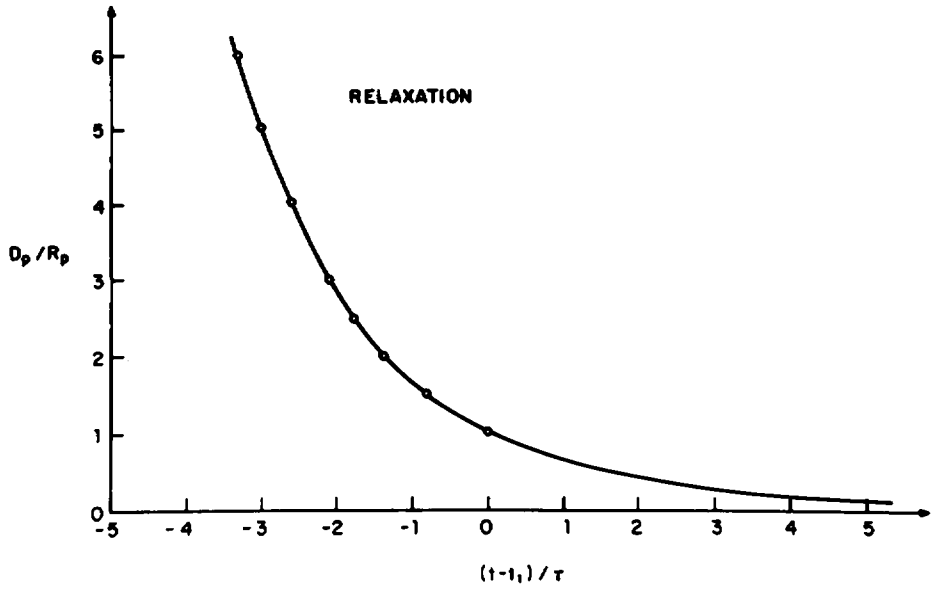

FIGURE 5 Combination of the theoretical relaxation curves with different D_{pm}/R_p values (Fig. 4). D_p/R_p is plotted against $(t - t_1)/\tau$.

The approximation described above for the loading phase (Eq. 22) may also be used for the relaxation phase. One obtains

$$ax + b + 4\tau\dot{x} = 0. \tag{27}$$

Integrating Eq. 27 gives

$$t = (4/a)\tau \ln[(ax_m + b)/(ax + b)] \tag{28}$$

where $4/a = 1.633$. Eq. 28 leads to

$$t - t_1 = -1.633\tau \ln[(ax + b)/(a + b)]. \tag{29}$$

Points computed by Eq. 29 are superimposed on the exact curves of Eq. 25 in Fig. 5. This approximate solution leads to an exponential form which can be used to test the experimental data:

$$(x - 0.245)/(x_m - 0.245) = e^{-t/1.633\tau} \tag{30}$$

where -0.245 is equal to b/a.

EXPERIMENTAL METHODS

The Micropipette and Pressure Regulating System

Micropipettes with internal radius (R_p) ranging from 0.3 to 0.8 μm were prepared with the use of micropipette puller (Narishige Scientific Instrument Laboratory, Tokyo). By the use of a slow pulling time (approximately 20 min), the internal radius was uniform for at least 4 μm

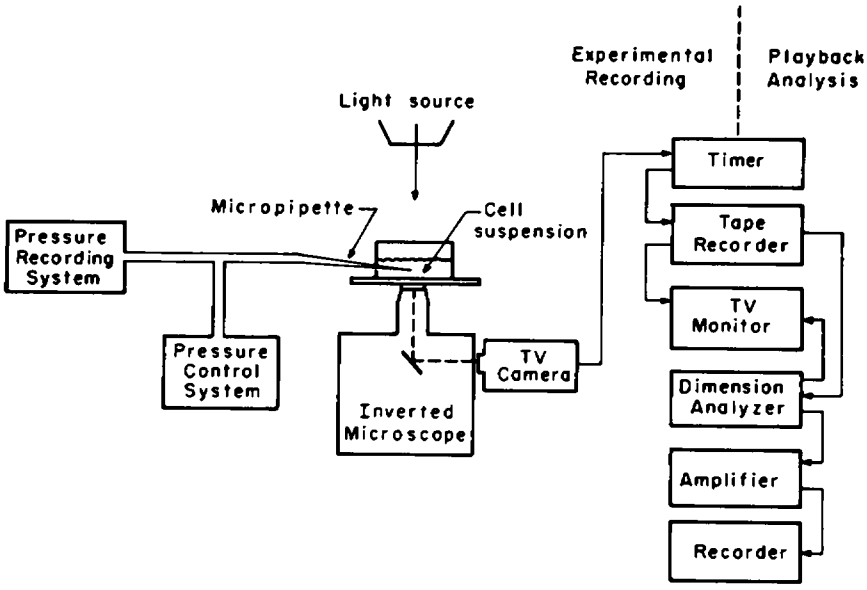

FIGURE 6 Schematic drawing showing the set-up for the micropipette experiment and for playback analysis.

from the tip. The micropipette was filled with a buffered saline-albumin solution, which contained 0.9 g/100 ml NaCl, 0.25 g/100 ml serum albumin, and 12 mM Tris, with the pH adjusted to 7.4 by the dropwise addition of 1 N HCl. The saline-albumin solution had an osmolality of 290–295 mosmol, and it had been filtered through a 0.2-μm membrane (Nalge Sybron Corp., Rochester, N.Y.) before usage. The filled micropipette was mounted on a micromanipulator (Narishige Scientific Instrument Laboratory), and the wide end of the pipette was connected to a pressure regulation system (Fig. 6).

The pressure regulation system has a damping chamber (approximately 10 ml total volume) partially filled with the saline-albumin solution, with which the filled micropipette is connected. The air phase of the damping chamber was connected through a three-way stopcock to the air phase of a partially filled water reservoir bottle, the liquid phase of which was connected to the liquid phase of another water reservoir bottle open to the atmosphere. The heights of both reservoir bottles were adjustable, and a micrometer indicator (Montgomery & Co., Chatham, N.J.) was used to control the height of the open bottle with an accuracy of better than 10 μm. By adjusting the relative heights of the two reservoir bottles, desired pressure levels can be preset and then imposed on the micropipette by turning the three-way stopcock to connect the closed reservoir bottle to the damping chamber and micropipette. The pressure level in the micropipette system was monitored by the use of a transducer (model 23BC, Statham Instrument, Inc., Oxnard, Calif.) and recorded with the use of an amplifier-recorder system (Gould Inc., Cleveland, Ohio). To minimize fluctuations in pressure reading when turning the stopcock, a layer of mineral oil was placed on top of the water in each reservoir bottle, and the air/liquid volume ratio in the damping chamber was adjusted to give a fast system response (time constant approximately 20 ms) without oscillation.

Preparation of Erythrocytes

Fresh blood samples were obtained from the antecubital vein of healthy human subjects (age 21–48 yr) with EDTA as the anticoagulant. After centrifugation at 1,500 *g* for 10 min, the

plasma and buffy coat were removed. The erythrocytes were washed twice in the buffered saline-albumin solution, and then suspended in the same solution at a volume concentration of approximately 0.03%. The prepared cells were studied as soon as possible, and the experiment was usually completed within 3 hr. Repeated testing during this period did not show any significant change with time.

Deformation and Recovery of Erythrocytes in the Micropipette

The erythrocyte suspension was loaded into a small round chamber (10 mm diameter and 8 mm height) located on the stage of a Nikon inverted microscope (Ehrenreich Photo-Optical Inc., Garden City, N.Y.). The chamber was covered to minimize evaporation. The erythrocytes were viewed through the bottom of the chamber with the use of an oil lens objective (100 ×, NA 1.25) and a 20 × eye piece. The image was also monitored and recorded with the use of a video camera and tape recorder system (Panasonic Co., Div. of Matsushita Electric Corp. of America, Franklin Park, Ill.) (Fig. 6). With the use of a K mirror, the image was rotated so that the micropipette axis is aligned with the television scan lines. The magnification of the system was calibrated with the use of a micron scale (50 × 2 μm, Graticules Ltd, Towbridge Kent, England). A video timer (model G-77, Odetics, Inc., Anaheim, Calif.) was used to record the date and the clock time on the video tape.

The micropipette tip was manipulated for positioning at the membrane surface of erythrocytes in its dimple region. With a slight change in micropipette pressure by using the micrometer control on the open reservoir bottle, the cell membrane can be either drawn toward the pipette tip (negative pressure) or pushed away (positive pressure). The zero pressure level was established when the cell membrane maintained its original position despite the presence of the micropipette tip at its surface. A desired level of negative pressure (ranging from -1 to -18 mm H_2O) was set in the reservoir system and then transmitted to the micropipette to cause a time-dependent aspiration of a portion of the cell. This step pressure was maintained for a predetermined period of time (usually 20 s). At the end of this period, the negative pressure was removed as a step function. This led to a time-dependent recession of the aspirated segment in the micropipette, ending in a total exit and shape recovery of the cell. The radius of the pipette used ranged from 0.3 to 0.8 μm. The use of the small pipette size, especially in experiments with greater aspirated length, served to minimize the membrane area and cell volume in the pipette and to reduce the probability of cell buckling. The volume aspirated into the pipette was always <5% of the cell volume.

Determination of the Time-Courses of Deformation and Recovery

The video image recorded on the tape was played back through a video dimension analyzer (Instrument for Physiology and Medicine, La Jolla, Calif.) and monitored on the television screen (Fig. 6). The video cursor lines of dimension analyzer were positioned along the axis of the micropipette, and the trigger zone was set as close as possible to the tip of the pipette.[4] Because of the difference in the video densities between the erythrocyte and the saline-albumin solution, the trigger zone traced the boundary of the cell during its deformational entry and its recession upon pressure release. The electrical output from the dimension analyzer was amplified and recorded (Gould, Inc.).

[4]When the trigger zone cannot be set precisely at the tip of the pipette, correction is made during analysis so that zero time corresponds to the time at which the trigger zone reaches the pipette tip.

RESULTS

The deformation and recovery of one erythrocyte as monitored by the use of the video dimension analyzer are shown in Fig. 7, where the ordinate D_p represents the length of the deformed erythrocyte segment inside the micropipette. A step-negative pressure was applied to induce the deformation by aspiration, and the aspiration pressure was removed as a step function 20 s later to allow the time-dependent recovery.

Steady-State Behavior: Membrane Elasticity

The steady state, maximum value of D_p was determined as D_{pm}, which is a function of the aspiration pressure applied (ΔP), the internal radius of the micropipette (R_p), and the elastic modulus of the cell membrane (μ). The steady-state stress-strain data (points in Fig. 8) obtained with the use of different values of ΔP and R_p were combined by plotting the dimensionless deformation parameter D_{pm}/R_p (ordinate in Fig. 8) against $\Delta P(R_p)$ (bottom abscissa in Fig. 8). The solid line in Fig. 8 is the theoretical relation between D_{pm}/R_p and the dimensionless membrane tension parameter $\Delta P(R_p)/\mu$ (top abscissa) (Eq. 17). Our experimental data can be fitted to this theoretical curve if the value of 4.2×10^{-3} dyn/cm is used for μ. The value of μ for each

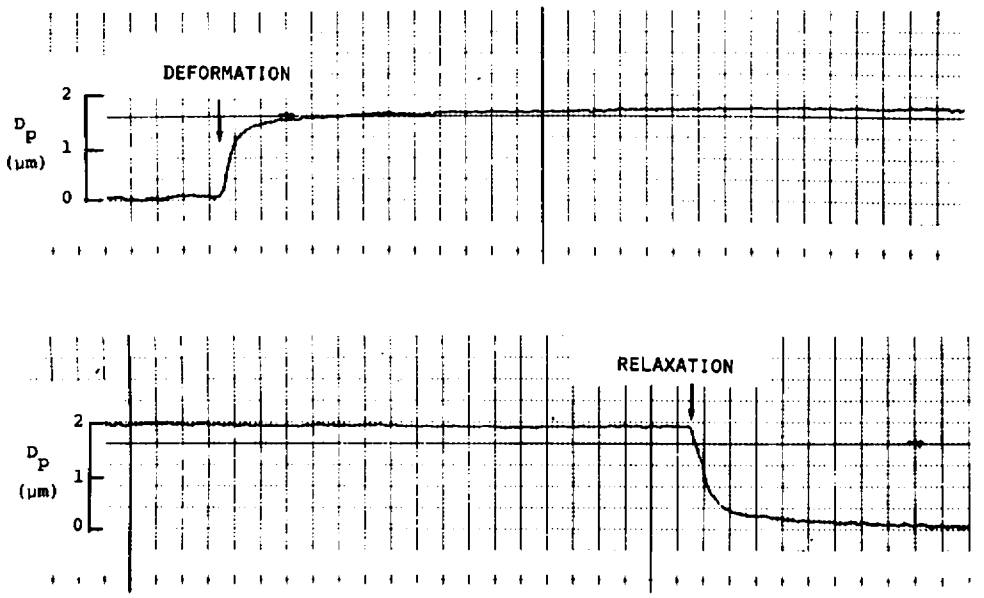

FIGURE 7 Records obtained from the video dimension analyzer showing the time-course of the deformational entry of a portion of an erythrocyte into a micropipette (R_p = 0.7 μm) after the application of an aspiration pressure of −5 mm H_2O (upper panel) and the time-course of relaxation after the removal of the aspiration pressure. The time interval between fine vertical lines is 40 ms. A slow chart speed was used to obtain this record to show the slow deformation phase. A faster chart speed was employed for the detailed analysis of the rapid deformation phase.

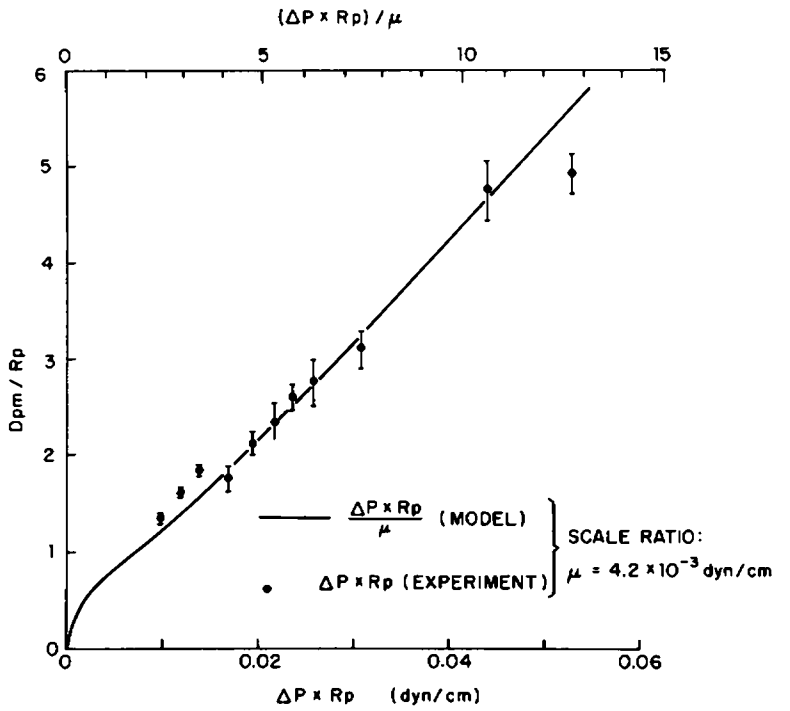

FIGURE 8 The steady-state dimensionless deformation (D_{pm}/R_p) of normal human erythrocyte membrane plotted against $\Delta P(R_p)$ (top abscissa) and the dimensionless membrane tension $\Delta P(R_p)/\mu$ (bottom abscissa), with the use of 4.2×10^{-3} dyn/cm for μ. The solid curve is the theoretical relationship derived from the spherical cap model (Eq. 17).

data point can also be calculated by comparing the experimental value of $\Delta P(R_p)$ and the theoretical value of $\Delta P(R_p)/\mu$ at the given D_{pm}/R_p. The results indicate that μ does not show a significant dependence on D_{pm}/R_p or $\Delta P(R_p)$.

Time-Dependent Deformation in the Micropipette: Membrane Viscoelasticity during Loading

The deformational entry of the erythrocyte into the micropipette in response to a step aspiration pressure exhibits a two-phase behavior (Fig. 7). After an initial rapid phase of deformation, which is considerably shorter than 1 s, there was a continued, slower phase of deformation, with the final D_{pm} value attained within the 20-s period of experimental observation. The time-dependent behavior of the deformation in the initial rapid phase was analyzed by taking the first plateau D_p value (attained in <1 s) as D'_{pm}.[5] The slope of the line relating $\ln(D'_{pm} - D_p)$ to time (Fig. 9) is inversely re-

[5]This D'_{pm} value was obtained by plotting $\ln(D_{pm} - D_p)$ against time and drawing a line to fit the slow phase. The point at which this slow phase line departs from the original curve is identified, and the D_p value for this point is taken as the D'_{pm}. To test the reliability of D'_{pm} value obtained by such curve inspection, a series of different D'_{pm} values were used in some experiments and the relationship between $\ln(D'_{pm} - D_p)$ and time was analyzed. The best D'_{pm} value was chosen on the basis of (*a*) the highest coefficient of

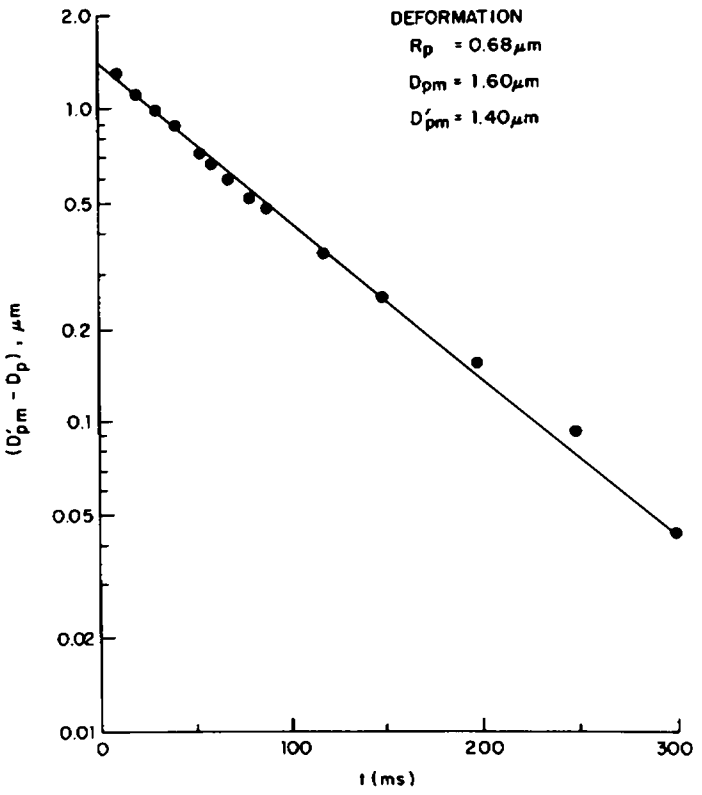

FIGURE 9 Graphic analysis of the time-dependent behavior of erythrocyte deformation. Plotting of $(D'_{pm} - D_p)$ on a semilogarithmic scale against time yields a single exponential line, from which the time constant of the rapid phase is determined.

lated to τ_{D_1}, the time constant of the rapid phase of deformation. According to Eq. 23,

$$\tau_{D_1} = -1/\{1.633\,[\mathrm{d}\ln(D'_{pm} - D_p)/\mathrm{d}t]\}. \tag{31}$$

The value of τ_{D_1} ranges from 0.018 to 0.115 s, and it shows an inverse relation with the degree of deformation, either measured as D'_{pm}/R_p or D_{pm}/R_p (Fig. 10).

The experimental data (open circles) on three erythrocytes subjected to different values of D'_{pm}/R_p are shown in Fig. 11, where D_p/R_p is plotted against the dimensionless time $(t - t_1)/\tau_{D_1}$. Also shown are the theoretical D_p/R_p versus $(t - t_1)/\tau_{D_1}$ curves (broken lines in Fig. 11, see Fig. 3), which agree well with the experimental curves at each of the three D'_{pm}/R_p levels. It is to be noted that the matching of the

correlation and (*b*) the agreement of intercept value obtained by linear regression with the D'_{pm} used. The D'_{pm} value obtained by such objective criteria agreed within 0.03 μm of the D'_{pm} value obtained by curve inspection.

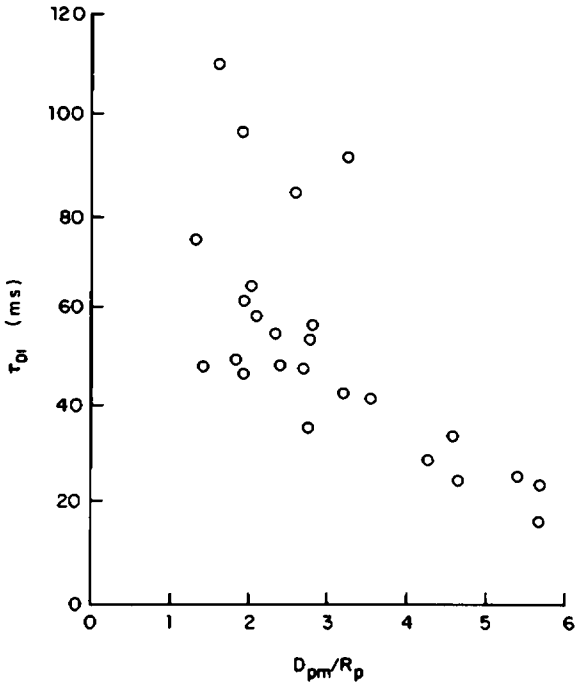

FIGURE 10 Variation of the time constant of the rapid phase of deformation (τ_{D_1}) with D_{pm}/R_p. Each point represents the mean of 4–6 cells, with a total of 120 cells studied.

theoretical and experimental results can be attained only by using the appropriate τ_{D_1} values, which varied inversely with D'_{pm}/R_p and covered a six-fold range.

The membrane viscosity during the rapid deformation phase (η_{D_1}) can be calculated as

$$\eta_{D_1} = \mu\tau_{D_1}. \tag{32}$$

η_{D_1} ranged from 0.6×10^{-4} to 4×10^{-4} dyn · s/cm and as τ_{D_1}, it varied inversely with D'_{pm}/R_p or D_{pm}/R_p (Fig. 12).

The slow deformation phase had a time constant (τ_{D_2}) of 5.04 ± 3.12 s (SD) and the membrane viscosity during the slow deformation phase (η_{D_2}) averaged 2.06×10^{-2} dyn · s/cm. Neither τ_{D_2} nor η_{D_2} showed significant correlation with the degree of deformation.

Time-Dependent Recovery in the Micropipette: Membrane Viscoelasticity during Unloading

When the aspiration pressure was removed, the deformed erythrocyte segment in the micropipette reduced its length with time (Fig. 7). Following Eq. 30, $\ln\{[(D_p/R_p) - 0.245]/[(D_{pm}/R_p) - 0.245]\}$ was plotted against time (Fig. 13). This yielded a single

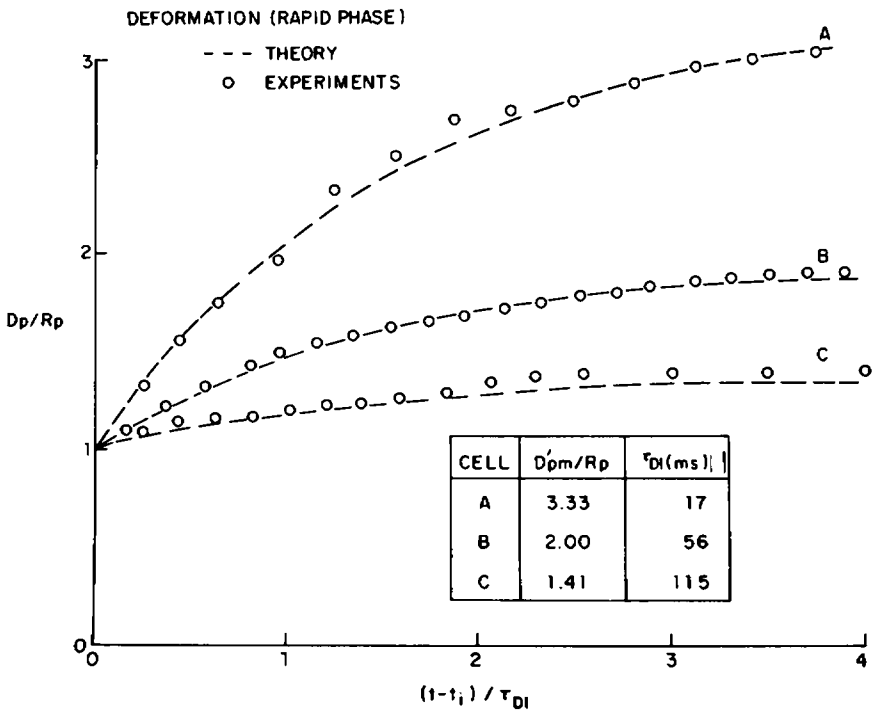

FIGURE 11 Experimental data on D_p/R_p (open circles) obtained on three erythrocytes subjected to different degrees of deformation (see D'_{pm}/R_p values in *inset*) plotted against dimensionless time $(t - t_1)/\tau_{D_1}$. These data points can be well matched with the theoretical curves (broken lines, from Eq. 18) only by the use of different τ_{D_1} values which vary inversely with the degree of deformation.

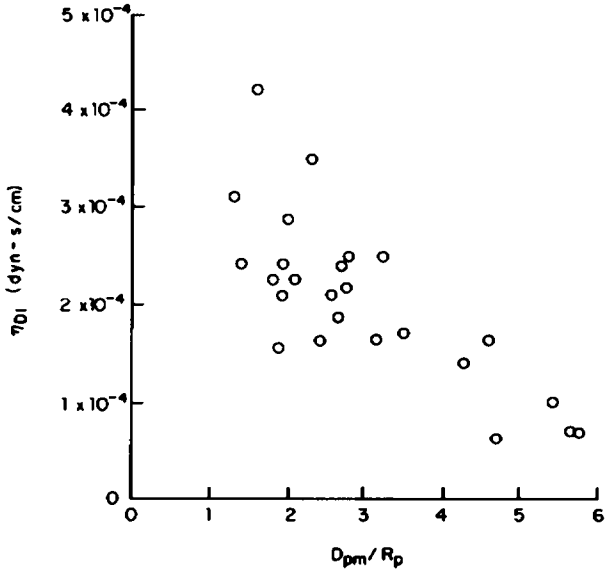

FIGURE 12 Variations in erythrocyte membrane viscosity during the rapid phase of deformation (η_{D_1}) with the degree of deformation (D_{pm}/R_p).

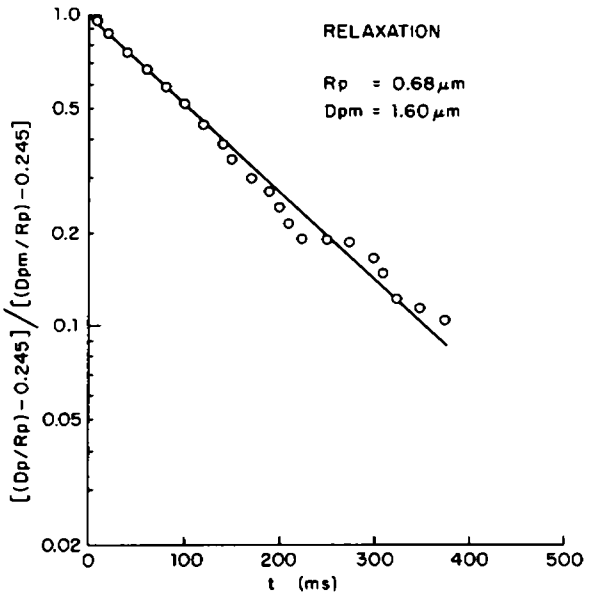

FIGURE 13 Graphic analysis of the relaxation of normal human erythrocyte membrane in the micropipette. The parameter $[(D_p/R_p) - 0.245)]/[(D_{pm}/R_p) - 0.245]$ (see Eq. 30) is plotted on a semilogarithmic scale against time. The time constant for recovery is determined from this monoexponential curve.

phase recovery, and the slope of the semilog plot is equal to $-1/1.633\tau_R$, where τ_R is the time constant during membrane recovery. The τ_R value averaged 0.146 ± 0.055 s (SD). The membrane viscosity during recovery (η_R) was calculated as

$$\eta_R = \mu\tau_R. \tag{33}$$

The η_R value averaged 5.44 ± 1.94 (SD) × 10^{-4} dyn · s/cm. Neither τ_R nor η_R showed significant correlation with the degree of deformation (Fig. 14). The experimental data (open circles) for three erythrocytes (same ones as in Fig. 11) subjected to different values of D_{pm}/R_p are shown in Fig. 15, where D_p/R_p is plotted against t/τ_R. Theoretical curves (broken lines in Fig. 15, see Figs. 4 and 5) agree well with these experimental results.

DISCUSSION

In the present micropipette experiments the steady-state relation between D_{pm}/R_p and $\Delta P(R_p)$ (Fig. 8) and the elastic modulus for normal human erythrocyte membrane (μ = 4.2 × 10^{-3} dyn/cm) agree in general with the results obtained by previous investigators (LaCelle et al., 1976; Waugh and Evans, 1976). Over the range of D_{pm}/R_p studied, μ does not vary with the degree of deformation.

The design of these experiments allowed dynamic quantitation of the time-dependent behavior of deformation as well as recovery of erythrocytes in the micropipette. The greater proportion of the deformation occurs in the initial, rapid phase, whereas the

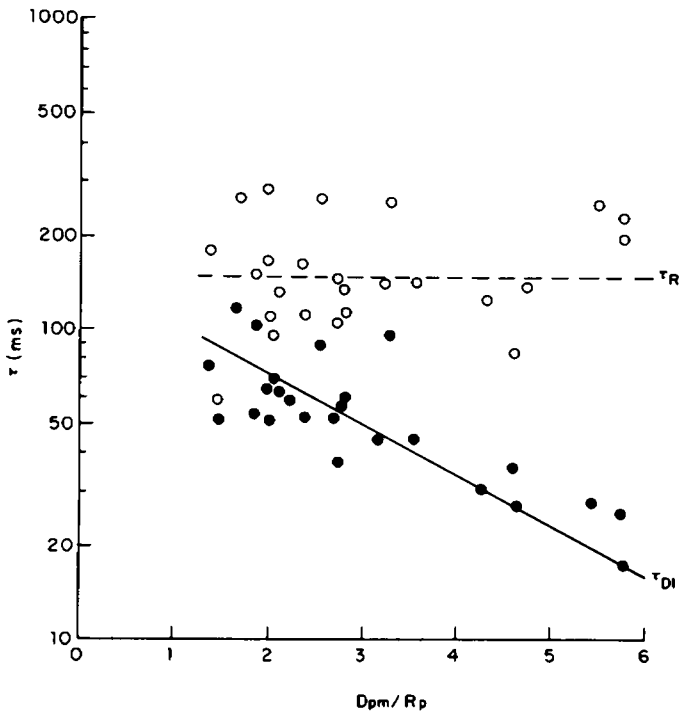

FIGURE 14 Semilogarithmic plot of time constants during recovery (τ_R, open circles) and during the rapid phase of deformation (τ_{D_1}, filled circles) against the degree of deformation (D_{pm}/R_p).

later, slow phase contributes to only a small fraction of the total deformation. The time constant of the rapid phase (τ_{D_1}) varies over a six-fold range and is related inversely to the dimensionless maximum aspiration (D'_{pm}/R_p or D_{pm}/R_p). Corresponding to the variation in τ_{D_1}, the membrane surface viscosity during rapid deformation (η_{D_1}) also has an inverse relation with D_{pm}/R_p. Increase in D_{pm}/R_p means an increase in the dimensionless pressure parameter $(\Delta P)R_p/\mu$ (Fig. 8). At the start of the deformation process, most of the pressure will be balanced by tension due to the viscous term in the constitutive equation if no initial elastic response is assumed as in Eq. 8. Strain rates V_{11} and V_{22} can be calculated from the experimental data on history of loading for each value of $(\Delta P)R_p/\mu$ as a function of time t. Comparisons made either at a given t or D_p/R_p indicate that V_{11} and V_{22} vary in the same direction as $(\Delta P)R_p/\mu$. This suggests that membrane surface viscosity η_{D_1} may decrease with increasing strain rate, i.e. a shear thinning behavior (Fig. 16). It should be pointed out, however, that η_{D_1} remains more or less uniform during the history of loading despite the changes of strain rates V_{11} and V_{22} with time. These two observations seem to be contradictory but may be reconciled if the membrane has memory of the loading history. It is possible that the initial strain rate may exert a shear thinning effect lasting over a certain period of time. Therefore, despite the progressive reduction

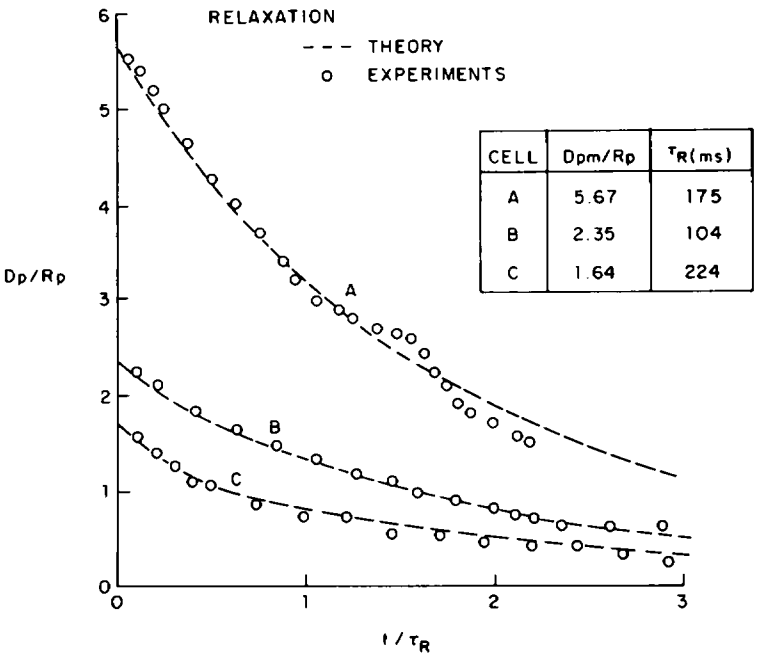

FIGURE 15 Experimental data on D_p/R_p (open circles) obtained on three erythrocytes (same as those in Fig. 11) during relaxation plotted against dimensionless time t/τ_R. These data points can be matched well with the theoretical curves (broken lines, from Eqs. 25 and A13) by the use of τ_R values which do not correlate with the degree of deformation.

in strain rate, the membrane behaves with essentially a constant viscoelastic property during the initial rapid deformation phase.

In comparison to the initial deformation, the slow deformation phase has a much longer time constant (τ_{D_2}) and a much higher membrane surface viscosity (η_{D_2}), neither of which varies with the degree of deformation. The value of η_{D_2} (2.06×10^{-2} dyn · s/cm) is more similar to the viscosity value observed during plastic deformation (Hochmuth et al., 1973; Evans and Hochmuth, 1976*b*).

The time constant (τ_R) of the recovery phase determined after 20 s of aspiration is independent of the degree of deformation, and the result agrees well with that of Hochmuth et al. (1977). The inverse relation between τ_{D_1} and the degree of cell deformation indicates that as D_{pm}/R_p or $(\Delta P)R_p/\mu$ approaches zero, τ_{D_1} rises to approach τ_R (Fig. 14). The constitutive equation used for the membrane leads to the same time constants for deformation and recovery. This condition is approached at very low D_{pm}/R_p levels. The large difference between τ_R and τ_{D_1} at high D_{pm}/R_p values suggests that the material properties of the erythrocyte membrane are altered during the 20-s period of deformation in the micropipette, with a consequent increase of the time constant. To test the possibility that a time-dependent change in membrane properties during the 20-s deformation period is responsible for the observed results, experiments have been conducted to study recovery after shorter periods of deformation. τ_R deter-

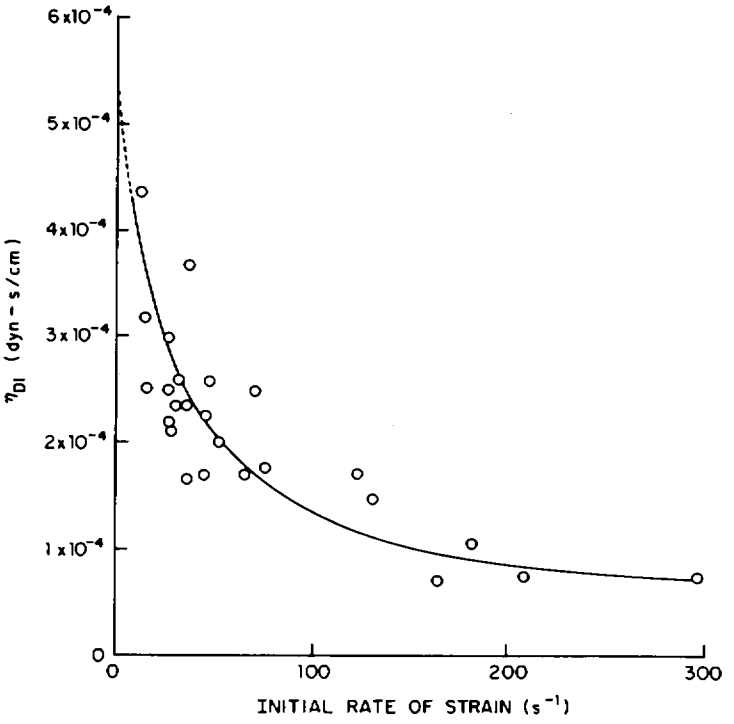

FIGURE 16 Membrane viscosity (η_{D_1}) during initial, rapid phase of deformation as a function of the initial rate of strain. As the initial rate of strain approaches 0, η_{D_1} approaches the value for η_R(5.4 x 10^{-4} dyn-s/cm).

mined after 2 s of deformation was indeed comparable to τ_{D_1} (Fig. 17); whereas τ_R after 5 s of deformation already showed a significant increase over τ_{D_1}, though the difference was not as striking as that observed after 20 s of deformation. The above discussions of τ values apply to the corresponding η values, as μ remains essentially constant under these conditions. These findings again demonstrate the importance of loading history on the rheological behavior of the membrane.

One possible way to explain the rather complicated viscoelastic behavior of the erythrocyte membrane is as follows: It is postulated that the molecular organization of the resting membrane is associated with a relatively high membrane surface viscosity. The high rate for deformation associated with a large D_{pm}/R_p leads to a loading configuration with a reduction of membrane surface viscosity (shear thinning). When the rate of deformation is slow, the membrane remains closer to the resting configuration with a high η. This would explain the inverse relation between η_{D_1} and D_{pm}/R_p (Fig. 12): The high η_{D_1} seen with slow rates of deformations reflects more closely the rheological properties of the membrane at rest, whereas the low η_{D_1} observed with high rates of deformation reflects the properties of the membrane that has been transformed to a loading configuration. The η_R values give an indication of

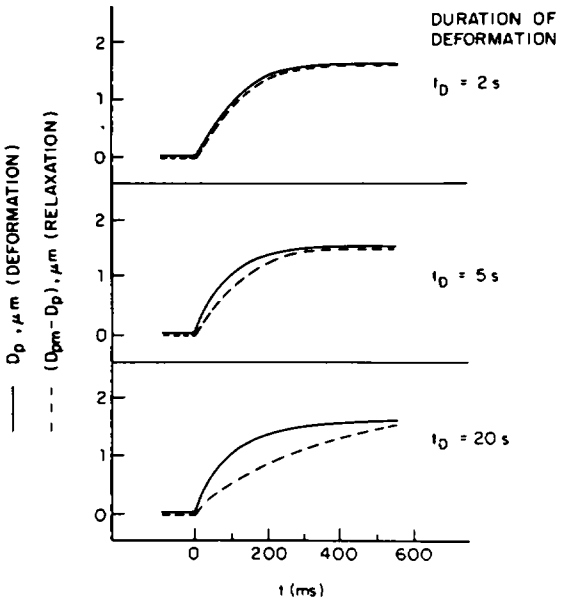

FIGURE 17 Comparison of time-courses of deformation and recovery of erythrocytes after various periods of deformation: (a) 2-s deformation; (b) 5-s deformation; (c) 20-s deformation. Solid lines: D_p in deformation phase; broken lines: $(D_{pm} - D_p)$ in recovery phase.

the properties of the membrane at the time of unloading, i.e., at the end of the step deformation period. After a 20-s deformation period, the η_R value does not show a dependence on the degree of deformation and is similar to the η_{D_1} value obtained at very small (or slow) deformations. Thus, during a prolonged deformation (e.g., 20 s), as the rate of deformation decreases, the molecular organization of the membrane probably returns from the loading configuration toward the resting configuration despite the presence of a continued deformation. Inasmuch as membrane properties seen during unloading agree rather closely with those seen during loading if the duration of deformation is short (e.g., 2 s, see Fig. 17), the return to the resting configuration seems to be a time-dependent phenomenon with a time constant of several seconds. The rheological behavior of the membrane seen during the slow phase may possibly reflect this slow process of returning to the resting configuration.

Another possible explanation for the slower time constant during relaxation than during loading is the hysteresis of membrane elasticity observed in quasi-steady state experiments (Waugh, 1977). However, the difference in apparent elastic moduli found for loading and unloading is only slightly over 10%, which would not be sufficient to account for the six-fold difference between τ_{D_1} and τ_R observed for the large D_{pm}/R_p experiments.

Our experiments also imply the absence of any static frictional force between the cell membrane and the pipettes. Because the thickness of this gap in the dynamic case

is below optical resolution, it is not possible to estimate accurately, but for the small surface areas and velocities involved, it appears that the fluid shear stresses are small.[6] Moreover, such stresses would be linear in the velocity and hence could not explain the highly nonlinear behavior observed.

In the present analysis on the rheological behavior of erythrocyte membrane, membrane bending stiffness has not been included. The bending properties may play a significant role in affecting the initial phase of cell deformation when D_p/R_p is less than unity.

The time constant for the rapid deformation phase (0.02–0.11 s) is considerably shorter than the mean transit time through a capillary vessel (approximately 0.5 s) as well as the cardiac cycle length (0.5–1 s). Therefore, each erythrocyte has sufficient time to undergo deformation in transit through the capillary vessel and may vary its degree of deformation with each cardiac cycle. The variation of τ_{D_1} with the loading condition (shear thinning) indicates that an increase in velocity through the micro-

[6] In addition to the viscous behavior of the cell membrane itself, there are several additional viscous losses which must be present to some extent. These should be small for the theory to be valid. These losses include a Poiseuille flow loss due to fluid movement in the pipette, shearing of the thin fluid layer between the cell membrane and the wall of the pipette, and the flow of hemoglobin into the pipette. It should be noted that after the hemoglobin enters the pipette, it moves as a rigid body and incurs no further loss. Hence the loss due to hemoglobin flow may be estimated as an orifice flow or the loss involved in half of a point sink flow down to the area of the pipette lumen.

The shearing of the fluid layer between the cell membrane and the pipette wall exerts a shear stress on the membrane so that during aspiration, the tension in the membrane at the tip of the pipette is reduced. This is equivalent to a reduction in the effective pressure applied.

To estimate typical magnitudes of the viscous losses, consider a case in which $x_m = 3$ at a time at which $x = 2$ in a pipette with $R_p = 0.5$ μm. The pipette diameter of 1 μm is assumed to be constant for 5 μm and then to expand with a 5° inclination of the tapered section. Under these assumptions, the length of contact between the pipette and the cell membrane is 0.5 μm axially and, allowing for 0.2 μm of pipette wall thickness, the total contact length is 0.7 μm. The fluid gap is estimated at 20 nm over this length. The fluid in the gap and in the pipette are assumed to have the same viscosity as water.

The values of x, x_m, and the dimensions assumed above lead to velocity $\dot{D}_p = 6.2$ μm/s using a time constant $\tau = 50$ ms from the experimental data. The mean velocity of the Poiseuille flow is then also 6.2 μm/s in the straight portion of the pipette and the total Poiseuille flow loss up to a 500-μm diamter is found to be 10.0 dyn/cm^2. The flow loss due to hemoglobin flow is based on a sink flow with a viscosity of 6 cP, but is only 0.7 dyn/cm^2 because it moves mainly as a rigid body. The loss due to the 20-nm film of fluid between the pipette and cell membrane is equivalent to a pressure drop of 8.6 dyn/cm^2. Thus the total of the fluid viscous losses is 19.3 dyn/cm^2. This is to be compared to the part of the applied pressure drop associated with the membrane viscosity. From Eq. 15, this is $\Delta P = 4\eta \dot{x}/R_p$ where $\eta = \mu\tau$. With the data assumed above and $\mu = 4.2 \times 10^{-3}$ dyn/cm, it is found that $\Delta P = 205$ dyn/cm^2. Thus the combined fluid losses are 9.4% of the membrane viscous loss. If a 50-nm film between the pipette and the cell membrane is assumed instead of a 20-nm film, the fluid loss drops to 6.9%. These percentages are a function of the geometry and fluid properties assumed, but are not dependent on the estimated velocity because all viscous terms are linear in the velocity. It may be concluded that fluid viscous losses are generally $<10\%$ of the membrane viscous loss.

For comparison, it may be noted that by cyclic, quasi-static tests, Waugh (1977) has estimated a hysteresis effect in similar pipette experiments on erythrocytes. The static friction may give an error of up to 13% in the computed elastic modulus. In this case, a static friction is compared to the elastic stress in the membrane. It may be expected that the dynamic fluid friction estimated here is less than the static friction, as this is generally the case, so that the present estimates appear reasonable by this comparison.

vessels would be accompanied by a faster deformation, thus ensuring the passage of the normal deformable cell.

The time constant for cell recovery may be relevant to the bulk viscometric behavior of concentrated erythrocyte suspensions (Chien, 1975). At low shear rates ($\dot{\gamma}$, e.g., $\dot{\gamma}$ below 1 s^{-1}), the time scale of shearing is sufficiently long ($1/\dot{\gamma}$ above 1 s) for the cells to recover their resting shape, and they behave essentially as rigid particles with a high suspension viscosity. At high shear rates (e.g., $\dot{\gamma}$ above 100 s^{-1}), the time scale of shearing is too short ($1/\dot{\gamma}$ below 0.01 s) for significant recovery to occur. This causes the cells to remain in a continuously deformed state as they slide by each other, resulting in a low suspension viscosity. The time constant for cell recovery averages 0.15 s, and this corresponds to a shear rate of approximately 6 s^{-1}. At this shear rate, the shear thinning behavior of suspensions of normal erythrocytes in nonaggregating medium is quite prominent (Chien, 1975). In blood flow through a cylindrical vessel, such as the venule, the shear rate is low in the center of the vessel. Therefore, erythrocytes have time to relax, and the interaction of the undeformed cells in the center of the tube causes the flattening of the velocity profile seen in these vessels (Schmid-Schönbein and Zweifach, 1975).

APPENDIX

In the spherical cap model described in the text, the theoretical treatment of the time-dependent deformation and relaxation of human blood cells in micropipette aspiration experiments was limited to conditions of $D_p/R_p \geq 1$. These analyses can be extended to smaller D_p/R_p (i.e., x) values by assuming that the portion of the cell in the micropipette takes on the shape of a spherical cap with various radii of curvature (r) as indicated in Fig. A1. Thus,

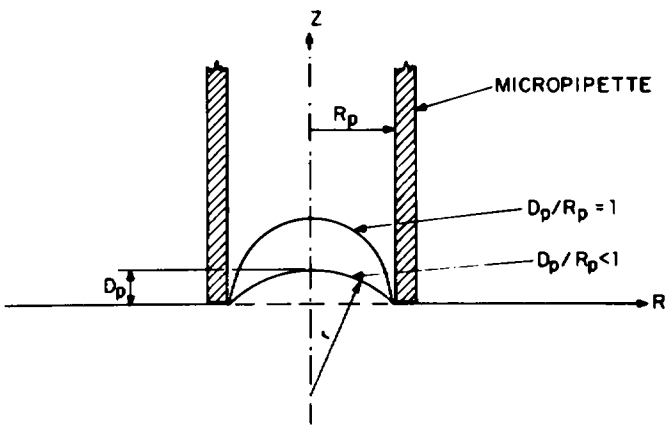

FIGURE A1 Schematic drawing to show the spherical cap model used to describe the aspirated portion of the cell into the micropipette. For small deformations, i.e., aspirated segment length (D_p) $\leq R_p$, the portion of the cell in the micropipette takes on the shape of a spherical cap with various radii of curvature (r).

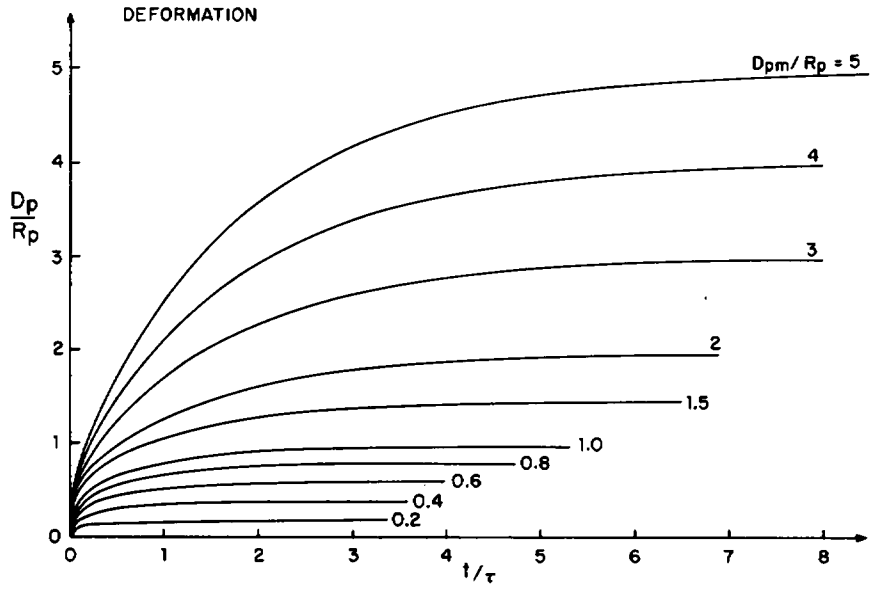

FIGURE A2 Theoretical modeling of time-dependent deformation of erythrocytes into the micropipette. Dimensionless deformation (D_p/R_p) as a function of dimensionless time t/τ. A family of curves with D_{pm}/R_p = 0.2–5 are shown.

For $x < 1$,

$$A = R_p^2 + D_p^2 \tag{A1}$$

$$A = 2D_p\dot{D}_p \tag{A2}$$

$$r = R_p[x + (1/x)]/2 \tag{A3}$$

and

$$T_{11}^0 = r\Delta P/2. \tag{A4}$$

Substitution of Eqs. A1–A4 into Eq. 14 yields

$$(\Delta P)R_p/\mu = 2[x^2 + \ln(1 + x^2)]x/(1 + x^2) + 8\tau\dot{x}x^2/(1 + x^2). \tag{A5}$$

For the steady-state equilibrium position, when x_m is reached ($x_m < 1$),

$$(\Delta P)R_p/\mu = 2[x_m^2 + \ln(1 + x_m^2)]x_m/(1 + x_m^2). \tag{A6}$$

In this case, Eqs. A5 and A6 can be used to find the time t to reach any $x \leq x_m$:

$$t = \tau \int_0^x \frac{dx}{F_1(x)} \tag{A7}$$

where

$$F_1(x) = \frac{1}{4x}\left\{\frac{1 + x^2}{1 + x_m^2}\frac{x_m}{x}[x_m^2 + \ln(1 + x_m^2)] - [x^2 + \ln(1 + x^2)]\right\} \tag{A8}$$

If $x_m \geq 1$, the time required to reach a given x is solved in two parts: The part of $x \geq 1$ is given in the text (Eq. 18), and the part for $x < 1$ is described by

$$t = \tau \int_0^x \frac{dx}{F_2(x)} \tag{A8}$$

where

$$F_2(x) = \frac{1}{4x}\left\{\frac{1 + x^2}{2x}(2x_m - 1 + \ln 2x_m) - [x^2 + \ln(1 + x^2)]\right\}. \tag{A9}$$

For the relaxation phase, if $x_m < 1$

$$\frac{\mu}{2}[x^2 + \ln(1 + x^2)] + 2\eta\dot{x}x = 0 \tag{A10}$$

and the history of relaxation is given by

$$t = \tau \int_x^{x_m} \frac{dx}{G_1(x)} \tag{A11}$$

where

$$G_1(x) = [x^2 + \ln(1 + x^2)]/4x. \tag{A12}$$

For $x_m \geq 1$ and $x < 1$, the relaxation will be given by Eq. A12 with appropriate limits:

$$t - t_1 = \tau \int_x^1 \frac{dx}{G_1(x)} \tag{A13}$$

For $x_m \geq 1$ and $x \geq 1$, the history of relaxation can be given by Eq. 25. The relaxation curves for different x_m values (Eqs. 25, A11, and A13) can be reduced to one single curve as shown in Fig. 5.

This investigation was supported by National Heart, Lung, and Blood Institute grant HL 16851.

Received for publication 21 February 1978 and in revised form 30 June 1978.

REFERENCES

CHIEN, S. 1975. Biophysical behavior of red cells in suspensions. *In* The Red Blood Cells. Vol. 2. D. Mac N. Surgenor, editor. Academic Press, Inc., New York. 2nd edition. 1031–1133.

CHIEN, S. 1977. Principles and techniques for assessing erythrocytes deformability. *Blood Cells.* **3**:71–99.

EVANS, E. A. 1973*a*. A new material concept for the red cell membrane. *Biophys. J.* **13**:926–940.

EVANS, E. A. 1973*b*. New membrane concept applied to the analysis of fluid shear and micropipette-deformed red blood cells. *Biophys. J.* **13**:941–956.

EVANS, E. A., and R. M. HOCHMUTH. 1976*a*. Membrane viscoelasticity. *Biophys. J.* **16**:1–11.

EVANS, E. A., and R. M. HOCHMUTH. 1976*b*. Membrane viscoplastic flow. *Biophys. J.* **16**:13–16.

EVANS, E. A., and R. M. HOCHMUTH. 1977. A solid-liquid composite model of the red cell membrane. *J. Membr. Biol.* **30**:351–362.

EVANS, E. A., and P. L. LACELLE. 1975. Intrinsic material properties of the erythrocyte membrane indicated by mechanical analysis of deformation. *Blood.* **45**:29–43.

HOCKMUTH, R. M., N. MOHANDAS, and P. L. BLACKSHEAR, JR. 1973. Measurement of the elastic modulus for red cell membrane using a fluid mechanical technique. *Biophys. J.* **13**:747–762.

HOCHMUTH, R. M., P. R. WORTHY, and E. A. EVANS. 1977. Surface viscosity of red cell membranes. Presented at the 70th Annual American Institute of Chemical Engineers Meeting, 18 November 1977. To be published in an *AIChE Symposium.*

HOEBER, T. W., and R. M. HOCHMUTH. 1970. Measurement of red cell modulus of elasticity by *in vitro* and model cell experiments. *J. Basic Eng.* **92**:604–609.

KATCHALSKY, A., O. KEDEM, C. KLIBANSKY, and A. DEVRIES. 1960. Rheological considerations of the haemolysing red blood cell. *In* Flow Properties of Blood and Other Biological Systems. A. L. Copley and G. Stainsby, editors. Pergamon Press, Inc., Elmsford, N.Y. 155–164.

LACELLE, P. L., R. I. WEED, and P. A. SANTILLO. 1976. Pathophysiologic significance of abnormalities of red cell shape. *In* Membranes and Disease. L. Bolis, J. F. Hoffman, and A. Leaf, editors. Raven Press, New York. 1–17.

RAND, R. P. 1964. Mechanical properties of the red cell membrane. II. Viscoelastic breakdown of the membrane. *Biophys. J.* **4**:303–316.

SCHMID-SCHÖNBEIN, G. W., and B. W. ZWEIFACH. 1975. RBC velocity profiles in arterióles and venules of the rabbit omentum. *Microvasc. Res.* **10**:153–164.

SCHMID-SCHÖNBEIN, H. 1976. Microrheology of erythrocytes, blood viscosity, and the distribution of blood flow in the microcirculation. *In* International Review of Physiology and Cardiovascular Physiology. II. Vol. 9. A. C. Guyton and A. W. Cowley, editors. University Park Press, Baltimore. 1–62.

SINGER, S. J. 1974. Molecular organization of membranes. *Annu. Rev. Biochem.* **43**:805–833.

SKALAK, R. 1973. Modeling the mechanical behavior of red blood cells. *Biorheology.* **19**:229–238.

SKALAK, R. 1976. Rheology of the red blood cell membrane. *In* Microcirculation. J. Grayson and W. Zingg, editors. Vol. I. Plenum Press, New York. 53–70.

SKALAK, R., A. TÖZEREN, R. P. ZARDA, and S. CHIEN. 1973. Strain energy function of red blood cell membranes. *Biophys. J.* **13**:245–264.

WAUGH, R. E. 1977. Temperature dependence of the elastic properties of red blood cell membrane. Ph.D. Thesis, Department of Biomedical Engineering, Graduate School of Duke University, Durham, N.C.

WAUGH, R. E., and E. A. EVANS. 1976. Viscoelastic properties of erythrocyte membranes of different vertebrate animals. *Microvasc. Res.* **12**:291–304.

WEISSMAN, G., and R. CLAIBORNE, editors. 1975. *Cell Membranes, Biochemistry, Cell Biology and Pathology.* HP Publishing Co., New York.